Check for updates

Proceedings of the ASME 2022
International Design Engineering Technical Conferences and
Computers and Information in Engineering Conference
IDETC-CIE2022
August 14-17, 2022, St. Louis, Missouri

DETC2022-91125

Downloaded from http://asmedigitalcollection.asme.org/IDETC-CIE/proceedings-pdf/IDETC-CIE2022/86304/V009T09A023/6943851/v009t09a023-detc2022-91125.pdf by Virginia Polytechnic Institute and State University user on 15 November 2022

BIFURCATION ANALYSIS OF A PD CONTROLLED MOTION STAGE WITH A NONLINEAR FRICTION ISOLATOR

Ehab E. Basta, Sunit K. Gupta, Oumar R. Barry*
Department of Mechanical Engineering
Virginia Tech, Blacksburg, Virginia 24061

ABSTRACT

The utilization of mechanical-bearing-based precision motion stages (MBMS) is prevalent in the advanced manufacturing industries. However, the productivity of the MBMS is plagued by friction-induced vibrations, which can be controlled to a certain extent using a friction isolator. Earlier works investigating the dynamics of MBMS with a friction isolator considered a linear friction isolator, and the source of nonlinearity in the system was realized through the friction model only. In this work, we present the nonlinear analysis of the MBMS with a nonlinear friction isolator for the first time. We consider a two-degree-of-freedom spring-mass-damper system to model the servo-controlled motion stage with a nonlinear friction isolator. The characteristic of the dynamical friction in the system is captured using the LuGre friction model. The system's stability and nonlinear analysis are carried out using analytical methods. More specifically, the method of multiple scales is used to determine the nature of Hopf bifurcation on the stability lobe. The analytical results indicate the existence of subcritical and supercritical Hopf bifurcations in the system, which are later validated through numerical bifurcation. This observation implies that the nonlinearity in the system can be stabilizing or destabilizing in nature, depending on the choice of operating parameters.

Keywords: Precision motion stage, LuGre model, method of multiple scales, Hopf bifurcation, Nonlinear friction isolator.

INTRODUCTION

Precision motion stages are used for high-speed precision positioning in advanced manufacturing and metrology-related processes (advanced machining, additive manufacturing, and semiconductor fabrications). Due to their wide range of motions, easy installation, cost-effectiveness, and high off-axis stiffness, the mechanical-bearing- based motion stages (MBMS) are more popular than their counterpart motion stages [1]. One or a combination of proportional (P), integral (I), and derivative (D) controllers are utilized to control the motion of MBMS [2, 3]. However, the application of servo controller in MBMS leads to the problem of self-excited limit cycles, also known as friction-induced vibrations (FIV), which further causes long settlings times, oscillations of tracking errors, and stick-slip phenomena [2, 4, 5]. Therefore, to mitigate the tracking error oscillation, which leads to better motion stage performance, it is vital to understand the dynamics of self-excited FIV under different conditions.

To mitigate or control the FIV, different controllers have been proposed; (1) model-based controllers, (2) high-gain controllers, and (3) advanced controllers (adaptive, model predictive, etc) [6–9]. Nevertheless, there can be certain limitations in the performance of these controllers. For instance, surrounding noise can limit high-gain controllers, model inaccuracy in the model-based controller, and low-performance computational/actuator hardware in the case of advanced controllers.

Recent studies [10, 11] developed a robust mechanical device known as the friction isolator (FI) to mitigate self-excited

*Address all correspondence to this author. Email: obarry@vt.edu

Copyright © 2022 by ASME

FIV in MBMS control systems. Since the compliant motion stages adopt FI as a motion-compliant joint between the bearings and the table, it efficiently isolates the table from the nonlinear effects of friction. Following these works, a detailed linear and nonlinear analysis was performed to identify key design parameters and operating conditions for stable operation of MBMS [12–14]. However, we emphasize that the above-mentioned studies investigate the dynamics of motion stages with linear FI, and did not consider the nonlinear dynamical components of FI. In practice, nonetheless, the mechanical design of FI can introduce nonlinear components that can be significant compared to the linear components. Therefore, we need to consider the nonlinearities from FI to understand the dynamics of compliant motion stages.

To the author's best knowledge, although the application of linear FI in MBMS is established, the nonlinear components of FI have not been considered in the analysis. Therefore, this study is believed to be the first to examine the dynamics of the motion stage with nonlinear FI. The LuGre friction model [15] is used to describe the friction dynamics between contact surfaces. The nonlinear analysis is performed using the method of multiple scales (MMS). The study shows that linear FI underestimates the linearly stable regime of operation. Also, we observe the existence of supercritical and subcritical Hopf bifurcations in the system depending on the selection of control parameters.

MATHEMATICAL MODEL OF MOTION STAGE

The mathematical model of the MBMS with nonlinear FI is briefly presented in this section. The current model is an extension of the model discussed in [14] and shown in Fig. 1. The motion stage is modeled as a rigid mass m_t, whereas the combined mass of the bearing and FI is modeled as m_b. The nonlinear spring with a stiffness function $g(.)$, and a linear damper with damping coefficient c_{fi} represent the interaction forces between m_b and m_t. Moreover, the input reference signal and output feedback control forces from the PD controller are denoted by $r(t)$ and u_1, respectively. Consequently, if $X_1(t)$ and $X_2(t)$ represent the position of precision motion stage and FI, respectively, then the governing equations of motion for the system can be written as

$$m_t\ddot{X}_1 + g\left(X_1 - X_2\right) + c_{fi}\left(\dot{X}_1 - \dot{X}_2\right) = u_1\,, \tag{1a}$$

$$m_b\ddot{X}_2 - g\left(X_1 - X_2\right) + c_{fi}\left(\dot{X}_2 - \dot{X}_1\right) = -F_f\,. \tag{1b}$$

where feedback force u_1 is defined as

$$u_1 = -k_p^* e - k_d^* \dot{e}\,. \tag{2}$$

In the above equation, k_p^* and k_d^* represent the proportional and differential gains, respectively, and the tracking error, e, is defined as the difference between the position and reference input. Moreover, in the governing equations of motion, the frictional force between the support platform and the bearing is denoted by F_f, and is modeled using the LuGre friction model [15]. In the LuGre model,

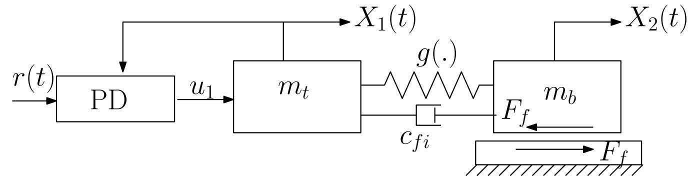

FIGURE 1: Schematic of PD controlled precision motion stage with nonlinear FI

microscopic degrees of freedom are incorporated by modeling asperities of the contact surfaces as elastic bristles with linear stiffness and viscous damping. Therefore, if z represents the average bristle deflection, the friction force in the LuGre model can be defined as

$$F_f = \sigma_0^* z + \sigma_1^* \dot{z} + \sigma_2^* V_r\,, \tag{3}$$

where σ_0^* and σ_1^* are the contact stiffness and the micro-damping of the bristle, respectively, σ_2^* is the macroscopic viscous friction between the contact surfaces, and V_r is the relative velocity between the two moving surfaces. In addition, the evolution of the average bristle deflection z with time is governed by [15, 16]:

$$\dot{z} = V_r - \frac{\sigma_0^*|V_r|}{g(V_r)} z = V_r\left(1 - \frac{\sigma_0^*\,\mathrm{sgn}(V_r)}{g(V_r)} z\right)\,, \tag{4}$$

where $g(V_r) > 0$ describes the Stribeck effect. For the analytical study of the system under investigation, we choose $g(V_r) > 0$ as [16],

$$g(V_r) = f_C^* + (f_S^* - f_C^*)e^{-(V_r/V_s)^2}\,, \tag{5}$$

where f_C^* is the Coulomb friction, f_S^* is the static friction, and $\tilde{a}$ is the slope parameter. Since earlier studies suggest that the nonlinearities involved with the LuGre friction model are primarily the combination of quadratic and cubic terms, we assume that stiffness function involved with friction isolator has similar nonlinear restoring force characteristic as our primary system, i.e., the combination of quadratic and cubic terms [17,18]. Therefore, provided that k_{fl}^*, k_{fq}^*, and k_{fc}^* represent the linear, quadratic, and cubic stiffness of FI, respectively, Eq. (1) can be written as

$$m_t\ddot{e} + k_p^* e + k_d^* \dot{e} + k_{fl}^*\left(e - e_b\right) + k_{fq}^*\left(e - e_b\right)^2 + k_{fc}^*\left(e - e_b\right)^3 + c_{fi}\left(\dot{e} - \dot{e}_b\right) = -m_t\ddot{e}\,, \tag{6a}$$

$$m_b\ddot{e}_b + k_{fl}^*\left(e_b - e\right) - k_{fq}^*\left(e_b - e\right)^2 + k_{fc}^*\left(e_b - e\right)^3 + c_{fi}\left(\dot{e}_b - \dot{e}\right) = -(\sigma_0^* z + \sigma_1^* \dot{z} + \sigma_2^* V_r) - m_b\ddot{e}_b\,. \tag{6b}$$

where e_b is defined as $e_b = X_2 - r$. We emphasize here that Eqs. (3), (4), (5), and (6) together govern the complete dynamics

Downloaded from http://asmedigitalcollection.asme.org/IDETC-CIE/proceedings-pdf/IDETC-CIE2022/86304/V009T09A023/6943851/v009t09a023-detc2022-91125.pdf by Virginia Polytechnic Institute and State University user on 15 November 2022

Copyright © 2022 by ASME

of the system. Consequently, to nondimensionalize the system, we define the following nondimensional parameters and scales:

$$x=\frac{e}{X_0}, x_b=\frac{e_b}{X_0}, \tilde{z}=\frac{z}{X_0}, X_0=\frac{g}{\omega_p^2}, \omega_p=\sqrt{\frac{k_p^*}{m_t}}, \tau=\omega_p t,$$
$$\zeta=\frac{k_d^*}{2m_t\omega_p}, v_r=\frac{V_r}{X_0\omega_p}, \sigma_0=\frac{\sigma_0^*}{m_t\omega_p^2}, \sigma_1=\frac{\sigma_1^*}{m_t\omega_p}, \sigma_2=\frac{\sigma_2^*}{m_t\omega_p},$$
$$f_c=\frac{f_c^*}{m_tX_0\omega_p^2}, f_s=\frac{f_s^*}{m_tX_0\omega_p^2}, a=\tilde{a}\omega_pX_0, \kappa=\frac{c_{fi}}{2m_t\omega_p},$$
$$k_r=\frac{k_{fi}}{k_p}, m_r=\frac{m_t}{m_b}, k_{rq}=\frac{k_{fq}^*X_0}{k_p^*}, k_{rc}=\frac{k_{fc}^*X_0^2}{k_p^*}.$$

Using the aforementioned non-dimensional scales and parameters with the assumption of constant reference velocity ($\ddot{r}=0$),, the nondimensional governing equations of motion can be rewritten compactly in state-space form as

$$\dot{x}_1=x_2\,, \tag{7a}$$

$$\begin{aligned}\dot{x}_2=&-2\zeta x_2-x_1-k_r\left(x_1-x_3\right)-k_{rq}\left(x_1-x_3\right)^2\\&-k_{rc}\left(x_1-x_3\right)^3-2\kappa\left(x_2-x_4\right)\,,\end{aligned} \tag{7b}$$

$$\dot{x}_3=x_4\,, \tag{7c}$$

$$\begin{aligned}\dot{x}_4=&-2\kappa m_r\left(x_4-x_2\right)-k_rm_r\left(x_3-x_1\right)\\&+k_{rq}m_r\left(x_3-x_1\right)^2-k_{rc}m_r\left(x_3-x_1\right)^3\\&-m_r\left(\sigma_0x_5+\sigma_1v_r\left(1-\frac{\sigma_0x_5}{g\left(v_r\right)}\mathrm{sgn}(v_r)\right)+\sigma_2v_r\right)\,,\end{aligned} \tag{7d}$$

$$\dot{x}_5=v_r\left(1-\frac{\sigma_0x_5}{g\left(v_r\right)}\mathrm{sgn}(v_r)\right)\,, \tag{7e}$$

with $[x_1,x_2,x_3,x_4,x_5]=[x(\tau),\dot{x}(\tau),x_b(\tau),\dot{x}_b(\tau),\tilde{z}(\tau)]$. If v_{rv} represents the non-dimensional constant reference velocity, the non-dimensional relative velocity v_r will be $v_r=\dot{x}_b+v_{rv}=x_4+v_{rv}$. We expand $1/g(v_r)$ in a Taylor series for small amplitude motion and keep terms till third order for the analytical treatment of our system with nonlinear FI to get

$$\frac{1}{g(v_r)}=\frac{1}{g(v_{rv}+x_4)}=g_0+g_1x_4+g_2x_4^2+g_3x_4^3\,. \tag{8}$$

where g_i are the same as defined in [16]. Next, a small parameter ε ($\varepsilon << 1$) is introduced in the governing equations by shifting origin of the solution to the equilibrium state as

$$x_i(\tau)=x_{is}+\varepsilon y_i(\tau)\,,\ (\text{for}\,i=1,2,...,5)\,, \tag{9}$$

where $y_i(\tau)$'s are the shifted coordinates. Thus, the equations of motion for our system in shifted coordinates can be written as

$$\dot{y}_1=y_2\,, \tag{10a}$$

$$\begin{aligned}\dot{y}_2=&-y_1-k_r\left(y_1-y_3\right)-2\zeta y_2-2\kappa\left(y_2-y_4\right)+h_1h_2\left(y_1\right.\\&\left.-y_3\right)+3h_1k_{rq}\left(y_1-y_3\right)-\varepsilon\left(y_3^2h_2-2y_3y_1h_2\right.\\&\left.+y_1^2h_2\right)-\varepsilon^2k_{rc}(y_1-y_3)^3\,,\end{aligned} \tag{10b}$$

$$\dot{y}_3=y_4\,, \tag{10c}$$

$$\begin{aligned}\dot{y}_4=&\alpha\,y_4h_4+g_0\,y_5\alpha\,\sigma_1\,v_{rv}\,\sigma_0+2\,\kappa\,\alpha\,\left(y_2-y_4\right)+y_1k_r\,\alpha\\&-y_3k_r\,\alpha-y_5\alpha\,\sigma_0+\left(3\,y_1\alpha\,h_1{}^2-3\,y_3\alpha\,h_1{}^2\right)k_{rc}\\&\left(-2\,y_1\alpha\,h_1+2\,y_3\alpha\,h_1\right)k_{rq}\\&+\varepsilon\left(y_4^2\left(-\alpha\,\sigma_1\,\sigma_2\,v_{rv}\,h_7+h_6\,h_7\right)-3\,k_{rc}\,\left(y_3-y_1\right)^2\alpha\,h_1\right.\\&\left.+k_{rq}\,\left(y_3-y_1\right)^2\alpha+y_4y_5\alpha\,\sigma_1\,\sigma_0\,h_5\right)+\varepsilon^2\left(-y_4^3\alpha\,\sigma_1\,h_0\,h_8\right.\\&\left.-y_4^2y_5\alpha\,\sigma_1\,\sigma_0\,h_7+k_{rc}\,\alpha\,\left(y_3-y_1\right)^3\right)\,,\end{aligned} \tag{10d}$$

$$\begin{aligned}\dot{y}_5=&-v_{rv}\,g_0\,\sigma_0\,y_5-g_1\,v_{rv}\,y_4h_0\\&-\varepsilon\left(g_0\,y_5y_4\sigma_0+y_5y_4v_{rv}\,g_1\,\sigma_0+y_4^2v_{rv}\,g_2\,h_0+y_4^2g_1\,h_0\right)\\&-\varepsilon^2\left(y_5y_4^2\sigma_0\,v_{rv}\,g_2+y_4^3v_{rv}\,g_3\,h_0+y_5y_4^2\sigma_0\,g_1+y_4^3g_2\,h_0\right)\,,\end{aligned} \tag{10e}$$

where $h_0=\frac{1}{g_0}$, $h_1=h_0+x_{s3}+\sigma_2v_{rv}$, $h_2=-3k_{rc}h_1+k_{rq}$, $h_3=h_1-x_{s3}-\sigma_2v_{rv}$, $h_4=-\sigma_2+\sigma_1g_1h_3v_{rv}$, $h_5=g_0+v_{rv}g_1$, $h_6=\alpha\sigma_1(h_1-x_{s3})$, $h_7=v_{rv}g_2+g_1$, and $h_8=g_2+g_3v_{rv}$. We emphasize that Eq. (10) has been divided by ε throughout to get the above perturbed nonlinear equations. Since nonlinearities in these equations appear as coefficients of higher orders of ε, the unperturbed system can be obtained by setting $\varepsilon=0$ in Eq. (10) for the linear stability analysis.

LINEAR AND NONLINEAR ANALYSIS

In this section, we present the linear and nonlinear analyses of our system. We first start with the linear stability, which provides the dynamical behavior of the system under small perturbation around the steady-states and the solution basis for the nonlinear analysis of the system.

Linear Analysis

The linearized system of equations can be obtained by setting $\varepsilon=0$ in (10) to get

$$\dot{y}_1=y_2\,, \tag{11a}$$

$$\begin{aligned}\dot{y}_2=&-y_1-k_r\left(y_1-y_3\right)-2\zeta y_2-2\kappa\left(y_2-y_4\right)\\&+h_1h_2\left(y_1-y_3\right)+3h_1k_{rq}\left(y_1-y_3\right)\,,\end{aligned} \tag{11b}$$

$$\dot{y}_3=y_4\,, \tag{11c}$$

Downloaded from http://asmedigitalcollection.asme.org/IDETC-CIE/proceedings-pdf/IDETC-CIE2022/86304/V009T09A023/6943851/v009t09a023-detc2022-91125.pdf by Virginia Polytechnic Institute and State University user on 15 November 2022

Copyright © 2022 by ASME

$$
\begin{aligned}
\dot{y}_4 =& m_r y_4 h_4 + g_0 y_5 m_r \sigma_1 v_{rv} \sigma_0 + 2\kappa m_r (y_2 - y_4) \\
&+ y_1 k_r m_r - y_3 k_r m_r - y_5 m_r \sigma_0 + \left(3 y_1 m_r {h_1}^2 \right. \\
&\left. -3 y_3 m_r {h_1}^2\right) k_{rc} + \left(-2 y_1 m_r h_1 + 2 y_3 m_r h_1\right) k_{rq}
\end{aligned} \tag{11d}
$$

$$
\dot{y}_5 = -v_{rv} g_0 \sigma_0 y_5 - g_1 v_{rv} y_4 h_0 . \tag{11e}
$$

The characteristic equation for the system is obtained by assuming the synchronous solution for y_i (for $i = 1,2,3,4,5$) and accordingly, substituting $y_i(\tau) = y_{i0} e^{\lambda\tau}$ in Eq. (11). Eventually, the solvability condition (the determinant of the coefficient matrix must vanish) leads to the system's characteristic equation. The roots of the characteristic equation determine the system's stability in the space of control parameters. If all roots lie in the left half of the complex plane, i.e., if all roots have a negative real part, then the system is linearly stable; otherwise, the system is linearly unstable.

Furthermore, if the system loses its stability due to the change in any of the control parameter values, a pair of complex conjugate roots cross the imaginary axis, i.e., ($\Re(\lambda = 0)$) and Hopf bifurcation occurs. Therefore, in the occurrence of Hopf bifurcation, we let $\lambda = i\omega$ for $\omega > 0$ in the characteristic equation, and accordingly, we separate real and imaginary parts as two algebraic equations. We solve for the nondimensional set point velocity signal, v_{rv} and nondimensional differential gain ζ in terms of other parameters and frequency ω. The appearance of exponential functions in v_{rv} makes them as transcendental simultaneous equations and difficult to get the analytical closed-form for $\zeta_{i,cr}$ and $v_{rv,cr}$. Therefore, these algebraic equations are solved numerically to get the critical values of nondimensional differential gain and reference velocity signal at the Hopf point.

Since the solution of the linearized equations of the system Eq. (11) will be a periodic solution at the Hopf point, it can be represented in terms of the eigenvectors as

$$
\mathbf{y}(\tau) = A_1 \mathbf{r}_1 \mathrm{e}^{i\omega\tau} + A_2 \mathbf{r}_2 \mathrm{e}^{-i\omega\tau} , \tag{12}
$$

where $\mathbf{y}(\tau) = [y_1(\tau), y_2(\tau), y_3(\tau), y_4(\tau), y_5(\tau)]^T$, A_1 and A_2 are the arbitrary complex conjugate constants, and $\mathbf{r}_1$ and $\mathbf{r}_2$ are the right eigenvectors of the characteristic matrix for the system corresponding to eigenvalues $\lambda = i\omega$ and $\lambda = -i\omega$ respectively. Next, the nonlinear analysis for our system using the method of multiple scales is presented.

Nonlinear Analysis Using The Method of Multiple Scales

The linear stability analysis of our system presented in the preceding subsection only helps us determine the time evolution of very small perturbations in stable and unstable regimes. Nevertheless, the existing nonlinearities in the system truly determine the sensitivity of steady states towards initial perturbations in a locally stable region and its time evolution. If all perturbations die out with time irrespective of their magnitude, then a locally stable region is considered a stable global region for the steady-states. If small perturbation dies out, nonetheless, and large perturbation settles down to the limit cycle, then the steady-states lose global stability. Therefore, the nature of the nonlinearity affects the dynamical characteristics of the system, and the nonlinear analysis of the system is an essential step towards understanding the system.

With the introduction of multiple time scales (T_0, T_1, T_2) in the system, the solution of our perturbed nonlinear equation (Eq. (10)) can be assumed to be a series in powers of ε till $\mathscr{O}(\varepsilon^2)$ and written as

$$
\begin{aligned}
\mathbf{y}(\tau) =& \mathbf{y}_0 (T_0, T_1, T_2) + \varepsilon \mathbf{y}_1 (T_0, T_1, T_2) + \varepsilon^2 \mathbf{y}_2 (T_0, T_1, T_2) \\
=& \mathbf{y}_0 + \varepsilon \mathbf{y}_1 + \varepsilon^2 \mathbf{y}_2 .
\end{aligned} \tag{13}
$$

where $\mathbf{y}(\tau) = [y_1(\tau),\, y_2(\tau),\, y_3(\tau),\, y_4(\tau),\, y_5(\tau)]^T$. In a next step, we perturb one of the control parameters from its critical value. This is done to understand the nature of nonlinearity and hence, the nature of Hopf bifurcation. In the current work, the nondimensional reference velocity, v_{rv} has been chosen as our bifurcation parameter, and accordingly, we perturb v_{rv} from its critical value as

$$
v_{rv} = v_{rv,cr} + \varepsilon^2 k_1 , \tag{14}
$$

where $v_{rv,cr}$ is the value of v_{rv} at the Hopf point with $\zeta = \zeta_{cr}$. Next, we substitute, Eqs. (13)-(14) in Eq. (10), and expand it in Taylor series for smaller values of ε. We get coupled ordinary differential equations by equating the coefficients of different orders of ε. For the sake of brevity and space constraints, these equations are not reported here.

Furthermore, we note that the equations corresponding to the order ε^0 are identical to the linearized unperturbed equations (Eq. (11)) with the control parameters at the Hopf point. Therefore, the solution for the equations at the order of ε^0 can be formulated as

$$
\mathbf{y}_0 (T_0, T_1, T_2) = A_1 (T_1 T_2) \mathbf{r_1} \mathrm{e}^{i\omega T_0} + A_2 (T_1 T_2) \mathbf{r_2} \mathrm{e}^{-i\omega T_0} . \tag{15}
$$

Notice that unlike the solutions for the linearized unperturbed equations, i.e., Eq. (11) where A_1 and A_2 complex numbers, A_1 and A_2 in Eq. (15) are now complex conjugate functions of slow time scales. Next, on substitution of the assumed form of the solution for y_0 in the equations corresponding to ε^1 and following [16] we get the slow flow equations as

$$
\frac{\partial R(T_2)}{\partial T_2} = q_{11} k_1 R + q_{12} R^3 , \frac{\partial \phi(T_2)}{\partial T_2} = q_{21} k_1 + q_{22} R^2 , \tag{16}
$$

where q_{11}, q_{12}, q_{21}, and q_{22} are functions of system and control parameters at the Hopf-point, and frequency. In addition, these equations serve as a tool to determine the nature of the Hopf-bifurcation. A detailed discussion on these slow flow equations and verification of our analytical approach with numerical simulation is presented in the next section.

Downloaded from http://asmedigitalcollection.asme.org/IDETC-CIE/proceedings-pdf/IDETC-CIE2022/86304/V009T09A023/6943851/v009t09a023-detc2022-91125.pdf by Virginia Polytechnic Institute and State University user on 15 November 2022

Copyright © 2022 by ASME

RESULTS AND DISCUSSION

This section presents the results ba linear analysis of the system based on t the previous sections. For the numeric sis, we have used the parameter values fore proceeding further and determining furcation using MMS, it is required to v sults (Eq. (16)). To validate our analyti the results from MMS, i.e., slow flow merical simulation of the system using 'ode45'. For this, we choose two differ $\zeta_{cr} = 0.11873$, $v_{rv} = 0.0495 < v_{rv,cr} =$ $v_{rv} = 0.09 < v_{rv,cr} = 0.1$, both in the ur to the Hopf point. These comparisons ar Fig. 3, it can be easily observed that the of the system from MMS matches very cal time response counterpart and hence approach.

TABLE 1: Dimensional and non-dimens the simulation.

m_t [kg]	1.5	k_p	
m_b [N-s/m]	0.75	X_0 [m]	
σ_0^* [N/m]	$2.2e^6$	σ_1^*,σ_2^*	
f_c^* [N]	5.1	f_s^* [N]	
ω_0 [rad/s]	115.5	κ	
σ_0	110	σ_1	
σ_2	0.0823	f_s	
f_c	0.35	a	

Having established the analytical next present the criticality of Hopf bif curves, i.e., the nature of Hopf bifurcatic ent values of critical control parameters. of Hopf bifurcation, we utilize the slow- as it determines the amplitude of limit c Hopf point. More specifically, if stable point exist in the unstable regime only supercritical in nature. The existence of cation further implies that the system i nonlinearity in the system is stabilizing in nature. However, if small-amplitude unstable limit cycles exist in the linearly stable regime, and then the Hopf bifurcation is considered subcritical, eventually resulting in loss of global stability. Hence, to determine the nature of Hopf bifurcation and the global stability of steady states, we need to determine the steady-state amplitude of limit cycles emerging from the Hopf point. These amplitudes of limit cycles can be determined by the nontrivial fixed points of the slow-flow equations ($\dot{R} = 0$) and given by $R = \sqrt{\dfrac{-q_{11}k_1}{q_{12}}}$.

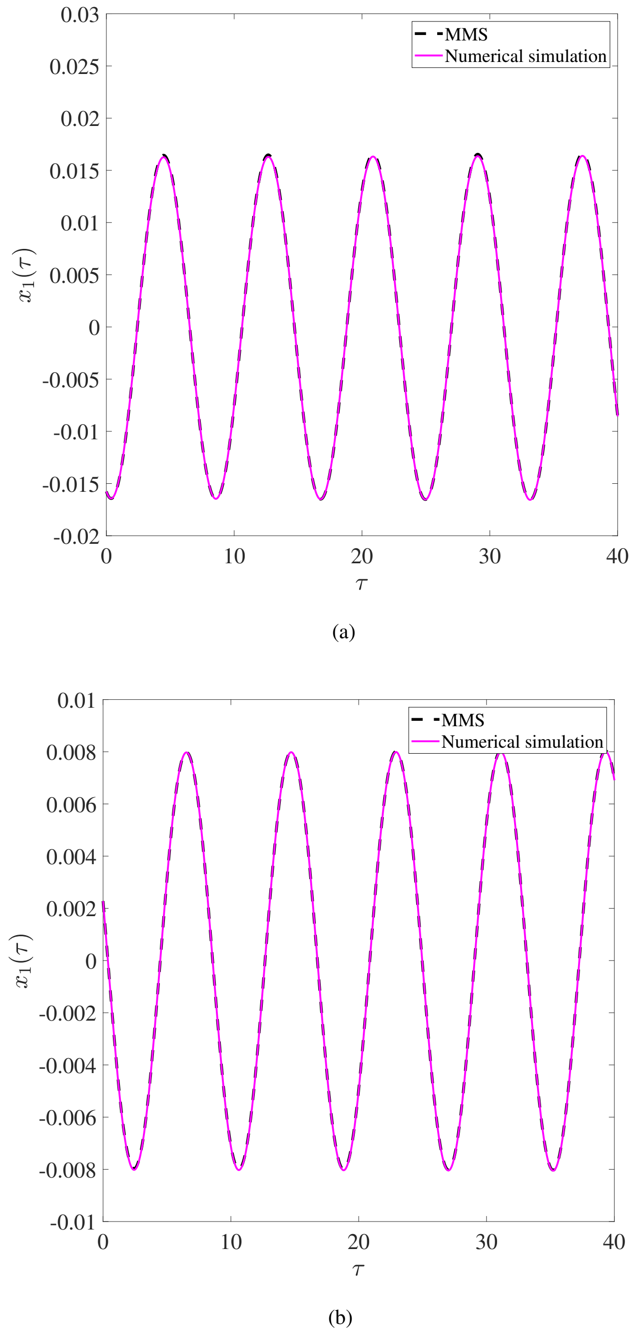

FIGURE 2: Comparison of time response of the system obtained from the MMS (dashed line) and numerical simulation (solid line) with (a) $\zeta_{cr} = 0.11873$, $v_{rv} = 0.04945 < v_{rv,cr} = 0.05$, (b) $\zeta_{cr} = 0.09502$, $v_{rv} = 0.088 < v_{rv,cr} = 0.1$, for the dynamics of PD controlled motion stage with nonlinear friction isolator. Other parameters are $\sigma_0 = 110$, $\sigma_1 = 1.37$, $\sigma_2 = 0.0823$, $f_s = 0.44$, $f_c = 0.35$, $\kappa = 0.001$, $a = 2.5$, $m_r = 2$, $k_{rq} = 0.22$, $k_{rc} = 0.22$, and $k_r = 0.5$.

Downloaded from http://asmedigitalcollection.asme.org/IDETC-CIE/proceedings-pdf/IDETC-CIE2022/86304/V009T09A023/6943851/v009t09a023-detc2022-91125.pdf by Virginia Polytechnic Institute and State University user on 15 November 2022

Copyright © 2022 by ASME

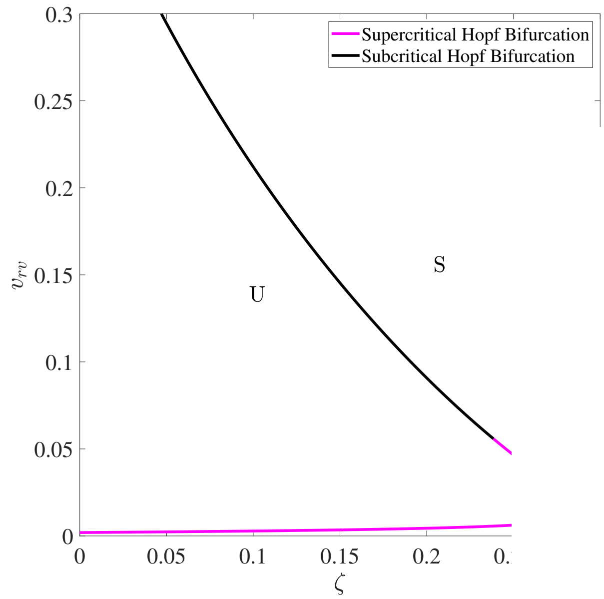

(a)

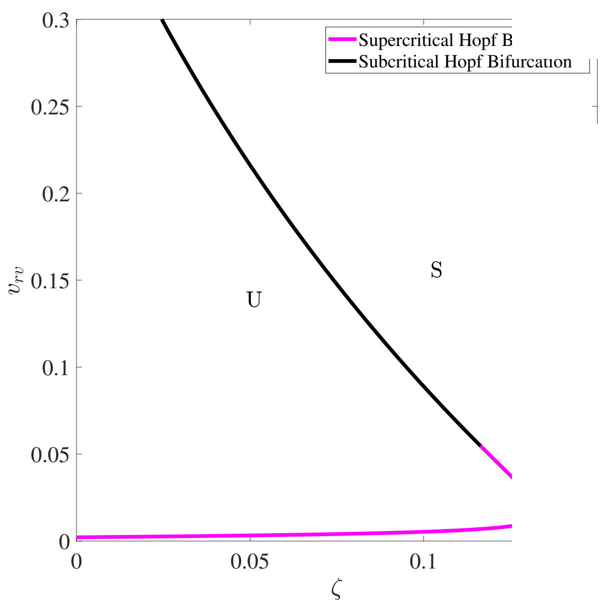

(b)

FIGURE 3: Criticality of Hopf bifurcation in th with (a) linear FI, and (b) nonlinear FI. Other $\sigma_0 = 110$, $\sigma_1 = 1.37$, $\sigma_2 = 0.0823$, $f_s = 0.44$, $f_c = 0.35$, $\kappa = 0.001$, $a = 2.5$, $m_r = 2$, and $k_r = 0.5$, $k_{rc} = 0.22$, and $k_{rq} = 0.22$.

Note that the quantity $q_{11}k_1$ is always positive in the linear unstable regime and negative in the linear stable regime, hence, the nature of Hopf-bifurcation is only governed by the sign of q_{12}. This observation implies that if q_{12} is negative, then limit cycles will exist in linearly unstable regimes only and the Hopf bifurca-

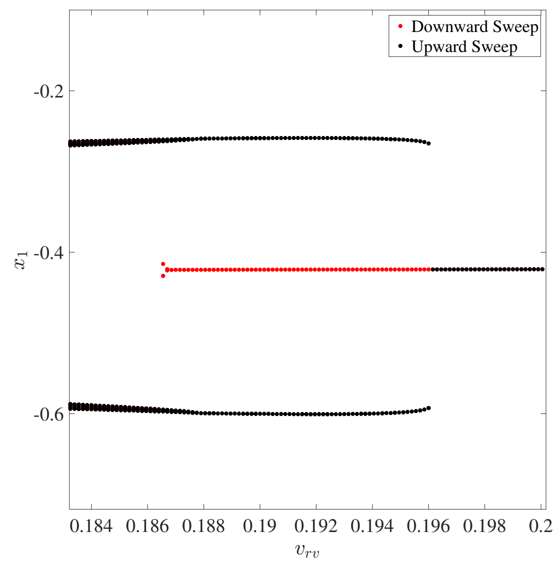

(a)

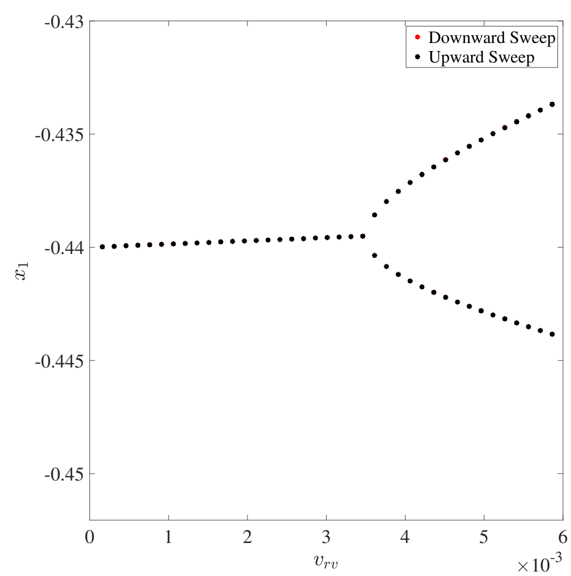

(b)

FIGURE 4: Numerical bifurcation diagram of motion stage with nonlinear FI with v_{rv} as bifurcation parameter showing (a) subcritical Hopf bifurcation, and (b) supercritical hopf bifurcation. Other parameters are $\sigma_0 = 110$, $\sigma_1 = 1.37$, $\sigma_2 = 0.0823$, $f_s = 0.44$, $f_c = 0.35$, $\kappa = 0.001$, $a = 2.5$, $m_r = 2$, $k_{rq} = 0.22$, $k_{rc} = 0.22$, and $k_r = 0.5$.

Downloaded from http://asmedigitalcollection.asme.org/IDETC-CIE/proceedings-pdf/IDETC-CIE2022/86304/V009T09A023/6943851/v009t09a023-detc2022-91125.pdf by Virginia Polytechnic Institute and State University user on 15 November 2022

Copyright © 2022 by ASME

tion will be supercritical in nature. However, if q_{12} becomes positive, then the limit cycles will also exist in the linear stable regimes, and the Hopf-bifurcation will be subcritical in nature. Therefore, the set of control parameters on the stability boundary corresponding to transition point from subcritical to supercritical or vice-versa can be found by setting $q_{12} = 0$.

Using this information, we plot the criticality of Hopf bifurcation on the stability plot in the parametric space of $\zeta - v_{rv}$ and shown in Fig. 3. The stable regime is marked by 'S' in the stability plot, while the unstable regime is marked by 'U'. Also, supercritical and subcritical Hopf bifurcations on these curves are marked with magenta and black colors, respectively. Figure 3 shows the criticality of Hopf bifurcation on the stability curve for the system with linear(Fig. 3a) and nonlinear FI(Fig. 3b). From Fig. 3, we can observe that for the given values of system parameters and nonlinear values of stiffness parameters, the inclusion of nonlinearity in the FI increases the local stability of the system significantly. However, nonlinear FI does not seem to improve the global stability of the system. For both systems, we observe that at low values of v_{rv}, supercritical Hopf bifurcations occur while steady states lose stability through subcritical Hopf bifurcations for high values of v_{rv}.

We employ and present the numerical bifurcation analysis to further validate our analytical findings of supercritical and subcritical bifurcations. For this numerical bifurcation analysis purpose, we have used built-in MATLAB routine 'ode45' with a high value of relative and absolute tolerance of '1e-13' to solve the five first-order systems of odes (Eq. (7)). These bifurcations diagrams, show the extrema of the error amplitude of motion stage, x_1 (corresponding to x_2=0), for motion stage with nonlinear FI and are shown in Fig. 4. These diagrams are plotted by fixing ζ and varying v_{rv} over a specified range in upward (increasing) and downward (decreasing) directions. From Fig. 4, we can observe that for a given value of ζ, at higher values of v_{rv} the stable limit cycles with steady-state solutions exist in the linearly stable regime, which implies that the Hopf bifurcation is subcritical in nature. On the other hand, for lower values of v_{rv}, stable limit cycles exist in the unstable region only, which indicates supercritical bifurcation. Both of the above-drawn observations are consistent with our analytical findings using MMS and further verify our analytical results.

We emphasize here that for a given value of primary system parameters, the inclusion of nonlinearity in dynamics of FI increases the local stability, while the global stability of the system does not change significantly. However, for other values of the system parameters and nonlinearities, it is possible to observe an enhanced region of global stability of the system is left for future work.

CONCLUSION

This work examined the nonlinear dynamics of a PD-controlled MBMS stage with a FI using analytical and numerical methods. The effects of nonlinearity from the friction isolator on the dynamics of motion stage were accounted for in this work for the first time, contrary to the earlier studies where the nonlinearity in the friction isolator was ignored entirely. The LuGre friction model was used to describe the dynamic effect of friction between the surfaces. Nonlinear analysis of the system was carried out using MMS. The analytical results showed an excellent match with the numerical simulation, hence, signifying the validity of the analytical approach. The criticality of Hopf bifurcation was plotted on the stability curves for given values of system and nonlinear parameters. We observed that the inclusion of nonlinearity increases the local stability of steady-states while global stability remains almost unchanged. Furthermore, we observed a transition of Hopf bifurcation from subcritical to supercritical or vice versa depending on the change in the value of the operating parameters for both systems, i.e., with linear FI and nonlinear FI. The validation of this criticality of Hopf bifurcation was done by performing numerical bifurcation analysis. We observed the existence of subcritical and supercritical Hopf bifurcation for higher and lower values of reference velocity signal and is consistent with analytical findings. A more detailed linear and nonlinear analysis of the system, which includes parametric analysis, exploration of the dynamics away from the Hopf point are left for future work.

ACKNOWLEDGEMENTS

This work is funded by National Science Foundation (NSF) CMMI #1855390: Towards a Fundamental Understanding of a Simple, Effective and Robust Approach for Mitigating Friction in Nanopositioning Stages; and CMMI #2000984: Nonlinear Dynamics of Pneumatic Isolators in Ultra-Precision Manufacturing Machines

REFERENCES

[1] Altintas, Y., Verl, A., Brecher, C., Uriarte, L., and Pritschow, G., 2011. "Machine tool feed drives". *CIRP annals*, ***60***(2), pp. 779–796.

[2] Futami, S., Furutani, A., and Yoshida, S., 1990. "Nanometer positioning and its micro-dynamics". *Nanotechnology*, ***1***(1), p. 31.

[3] Kim, M.-S., and Kim, J.-H., 2011. "Design of a gain scheduled pid controller for the precision stage in lithography". *International Journal of precision engineering and manufacturing*, ***12***(6), pp. 993–1000.

[4] Al-Bender, F., and Swevers, J., 2008. "Characterization of friction force dynamics". *IEEE Control Systems Magazine*, ***28***(6), pp. 64–81.

[5] Marques, F., Flores, P., Claro, J. P., and Lankarani, H. M.,

Downloaded from http://asmedigitalcollection.asme.org/IDETC-CIE/proceedings-pdf/IDETC-CIE2022/86304/V009T09A023/6943851/v009t09a023-detc2022-91125.pdf by Virginia Polytechnic Institute and State University user on 15 November 2022

Copyright © 2022 by ASME

2016. “A survey and comparison of several friction force models for dynamic analysis of multibody mechanical systems”. *Nonlinear Dynamics,* ***86***(3), pp. 1407–1443.

[6] Armstrong-Hélouvry, B., Dupont, P., and De Wit, C. C., 1994. “A survey of models, analysis tools and compensation methods for the control of machines with friction”. *Automatica,* ***30***(7), pp. 1083–1138.

[7] Maeda, Y., and Iwasaki, M., 2012. “Rolling friction model-based analyses and compensation for slow settling response in precise positioning”. *IEEE Transactions on Industrial Electronics,* ***60***(12), pp. 5841–5853.

[8] Dejima, S., Gao, W., Katakura, K., Kiyono, S., and Tomita, Y., 2005. “Dynamic modeling, controller design and experimental validation of a planar motion stage for precision positioning”. *Precision engineering,* ***29***(3), pp. 263–271.

[9] Yao, J., Deng, W., and Jiao, Z., 2015. “Adaptive control of hydraulic actuators with lugre model-based friction compensation”. *IEEE Transactions on Industrial Electronics,* ***62***(10), pp. 6469–6477.

[10] Dong, X., Yoon, D., and Okwudire, C. E., 2017. “A novel approach for mitigating the effects of pre-rolling/pre-sliding friction on the settling time of rolling bearing nanopositioning stages using high frequency vibration”. *Precision Engineering,* ***47***, pp. 375–388.

[11] Dong, X., and Okwudire, C. E., 2018. “An experimental investigation of the effects of the compliant joint method on feedback compensation of pre-sliding/pre-rolling friction”. *Precision Engineering,* ***54***, pp. 81–90.

[12] Dong, X., Okwudire, C., Wang, J., and Barry, O., 2019. “On the friction isolator for precision motion control and its dynamics”. In ASME 2019 International Design Engineering Technical Conferences and Computers and Information in Engineering Conference, American Society of Mechanical Engineers Digital Collection.

[13] Wang, J., Dong, X., Barry, O. R., and Okwudire, C., 2019. “Dynamical analysis of friction induced vibration in a precision motion stage with a friction isolator”. *arXiv preprint arXiv:1910.03212*.

[14] Gupta, S. K., Wang, J., and Barry, O. R., 2020. “Nonlinear vibration analysis of a servo controlled precision motion stage with friction isolator”. *International Journal of Non-Linear Mechanics*, p. 103554.

[15] De Wit, C. C., Olsson, H., Astrom, K. J., and Lischinsky, P., 1995. “A new model for control of systems with friction”. *IEEE Transactions on automatic control,* ***40***(3), pp. 419–425.

[16] Saha, A., and Wahi, P., 2014. “An analytical study of time-delayed control of friction-induced vibrations in a system with a dynamic friction model”. *International Journal of Non-Linear Mechanics,* ***63***, pp. 60–70.

[17] Habib, G., Detroux, T., Viguie, R., and Kerschen, G., 2015. “Nonlinear generalization of den hartog’s equal-peak method”. *Mechanical Systems and Signal Processing,* ***52***, pp. 17–28.

[18] Habib, G., and Kerschen, G., 2016. “A principle of similarity for nonlinear vibration absorbers”. *Physica D: Nonlinear Phenomena,* ***332***, pp. 1–8.

Downloaded from http://asmedigitalcollection.asme.org/IDETC-CIE/proceedings-pdf/IDETC-CIE2022/86304/V009T09A023/6943851/v009t09a023-detc2022-91125.pdf by Virginia Polytechnic Institute and State University user on 15 November 2022

 Copyright © 2022 by ASME